




Improvement of the thermal and mechanical properties of nature rubber composites by helical carbon nanofibers/ZnO hybrid

Yuming Li¹, Yongzhong Jin^{1,2,*} , Lin Pi^{1,2}, Xinglong Zheng¹, Wei Su^{1,2}, Cheng Wang³, and Jian Chen^{1,2}

¹ School of Materials Science and Engineering, Sichuan University of Science and Engineering, Zigong 643000, China

² Material Corrosion and Protection Key Laboratory of Sichuan Province, Zigong 643000, China

³ China Carbon Black Institute, Zigong 643000, China

Received: 7 July 2021

Accepted: 11 October 2021

Published online:
3 January 2022

© The Author(s), under exclusive licence to Springer Science+Business Media, LLC, part of Springer Nature 2021

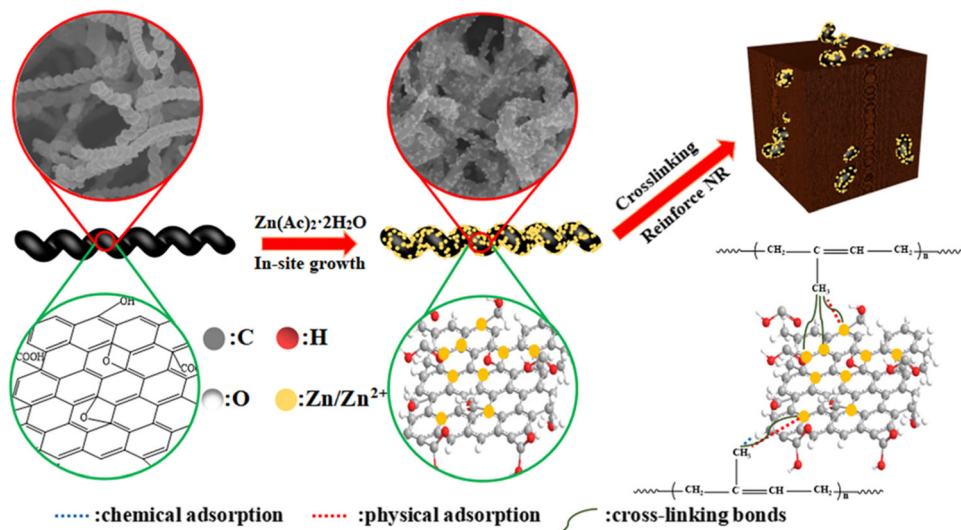
ABSTRACT

In the present work, helical carbon nanofiber-supported ZnO nanoparticles (HCNFs@ZnO) were synthesized via the in situ growth method. In the HCNFs@ZnO, ZnO nanoparticles exhibit an average size of ca. 30 nm and evenly anchor on the surface of HCNFs. With the incorporation of HCNFs@ZnO nanofiller into the nature rubber (NR), compared with the ZnO/NR composite (standard sample), the vulcanization rate, tensile strength, elongation at break, and modulus at 300% elongation of the HCNFs@ZnO/NR composite increase by 41%, 14%, 11%, and 6%, respectively. In addition, HCNFs@ZnO/NR composite also shows higher wet-skid resistance and lower rolling resistance compared with commercial ZnO/NR composite. The excellent performance of HCNFs@ZnO/NR composite should be ascribed to the fact that the HCNFs not only conduce to inhibiting agglomeration of ZnO nanoparticles but also serve as an efficient cure activator for sulfur vulcanization. This work showcases a simple route to develop novel ZnO nanofiller for high-performance nature rubber composites.

Handling Editor: Annela M. Seddon.

Address correspondence to E-mail: jyzcd@163.com

GRAPHICAL ABSTRACT



Introduction

Rubber composites have become one of the essential and irreplaceable materials for the national economy and daily lives, and been widely used in automotive tires, footwear, sealing elements, and so on [1–3]. To get sufficient properties, various types of fillers, such as ZnO, SiO_2 , and carbon black, must be added to reinforce rubber composites during sulfur vulcanization [4–6]. In this process, ZnO filler transforms to zinc polysulfide complexes through successive reactions with accelerator and sulfur and then bonds with rubber chains to produce a 3D network structure [7, 8]. Subsequently, ZnO filler is consumed continuously until the sulfur vulcanization completes [9–11]. Overall, ZnO filler as an activator not only saves the sulfur dosage and the curing time, but also improves the mechanical properties of rubber composite [12–14]. As is well known, nanostructuring can endow ZnO with a more reactive surface, thus further enhancing the crosslinking efficiency due to the maximization of the contact between ZnO and accelerators in rubber composite [11, 15–17]. However, it is vital to inhibit the agglomeration of ZnO nanoparticles during synthesis.

In recent years, compositing with carbon-supported materials, including carbon nanotubes (CNTs), microcrystalline cellulose (MCC), graphene oxide (GO), has become a universal strategy to improve the dispersion of ZnO nanoparticles for rubber manufacturing. For example, Liang et al. [18] adopted a microreactor technology to prepare MCC-ZnO hybrid by a microreactor technology. After adding 5 phr MCC-ZnO hybrids, the abrasion loss of the solution-polymerized styrene-butadiene rubber composite (SSBR2557A) could decrease from 0.76 to 0.34 cm^3 . Xu et al. [19] synthesized GO-ZnO hybrid by the method of electrostatic adsorption. Subsequently, the influences of GO-ZnO hybrid, GO + ZnO mixture, ZnO on the mechanical properties of chloroprene rubber composite (CR) were further investigated. It was found that GO-ZnO hybrid is an effective nanofiller for improving hardness, tensile strength, and modulus at 300% elongation of CR composite.

Apart from the excellent physical properties and the chemical resistance consistent with other carbon materials [20–22], helical carbon nanofibers (HCNFs) also display better elasticity and reversibility owing to their unique helical structure [23, 24]. In the previous work, HCNFs were successfully synthesized via a low-cost and simple catalytic chemical vapor

deposition (CCVD) [25]. In addition, HCNFs were also proved to be an effective rubber reinforcement by our follow-up work [26, 27]. To the best of our knowledge, however, there are no reports about the preparation of HCNFs-supported ZnO hybrid (HCNFs@ZnO) and its application in rubber composites.

Herein, we fabricated HCNFs@ZnO hybrid using zinc acetate dihydrate, diethylene glycol, HCNFs as starting materials via in situ growth method. Subsequently, the as-synthesized HCNFs@ZnO hybrid as nanofiller was used in the rubber composites. The HCNFs@ZnO hybrid not only enhanced vulcanization reaction but also improved mechanical properties of NR composite. The vulcanization rate, tensile strength, elongation at break, and modulus at 300% elongation of the HCNFs@ZnO/NR composite were higher than those of conventional ZnO/NR composite by 41%, 14%, 11%, and 6%, respectively. In addition, the HCNFs@ZnO/NR composite also exhibited excellent wet-skid resistance and low rolling resistance. Generally, a novel HCNFs@ZnO hybrid was developed in this work, which maybe is a prospective nanofiller for rubber composites.

Experimental section

Materials

Copper tartrate (purity > 99%) was pursued from Tianjin Kemeou Chemical Reagent Co. Ltd. Zinc acetate (ZA, purity > 99%), diethylene glycol (DG, purity > 99%), and carbon black N330 (CB, purity > 99%) were obtained from Chengdu Kelong Chemical Co. Ltd. Nature rubber (NR, purity > 92%), sulfur (S, purity 98%), commercial ZnO (c-ZnO, purity > 96%), stearic acid (SA), and 2,2'-dibenzothiazolesulfide (DM, purity > 99%) were supplied by China Carbon Black Institute.

Synthesis of HCNFs@ZnO hybrid

HCNFs were obtained through catalytic chemical vapor deposition (CCVD) according to our previous research [25]. The synthesis of HCNFs@ZnO hybrid with a mass ratio of 1:1 was described as follows. Firstly, 2.2 g ZA and 500 mL of DG were dissolved into 70 mL of deionized water and then heated at 170 °C in an oil bath until milky white appeared.

Afterward, the solution was kept for 12 h at room temperature. Subsequently, 0.5 g of HCNFs was added into the solution followed by ultrasonic oscillation for 20 min and then heated at 170–180 °C in an oil bath under stirring for 5 h. Next, the production was filtered and washed repeatedly with deionized water. Finally, the as-obtained black powder was treated in a tube oven at 150 °C for 2 h to remove impurities.

Preparation of HCNFs@ZnO/NR composites

Rubber composites were prepared by the mill-mixing method according to ADTM D 3192: 2005, as per Table 1. In the preparation process, the roller temperature was kept at 70 °C, and the total run time was maintained at 17 min. The pure NR was placed on a two-roller mill (model zg-200dr, China) and masticated for 2 min. Sequentially, 3 phr (parts per hundred of rubber) SA, 2.5 phr S, 0.6 phr DM, 5phr commercial microscale ZnO (c-ZnO), and 50phr CB were added. Finally, c-ZnO/NR composite (5/100) was obtained via refining according to the standard formula. According to the same procedure, the HCNFs@ZnO/NR composite (10/100) was prepared by using 10 phr HCNFs@ZnO replaced 5phr c-ZnO. For comparison, 5 phr and 10 phr HCNFs were added separately to prepare HCNFs/c-ZnO/NR (control, 5/100) and HCNFs/c-ZnO/NR (control, 10/100) and hereinafter referred to as HCNFs/NR (5/100) and HCNFs/NR (10/100).

Material characterization

Scanning electron microscope (SEM, Vega 3 SBU, Czech) was used to observe the surface morphologies of HCNFs and HCNFs@ZnO. Transmission electron microscope (Tecnai G2 F20 S-TWIN TMP, Netherlands) was used to observe the morphology of HCNFs and HCNFs@ZnO.

Thermogravimetry was conducted on a thermogravimetric analyzer (Q500, TA Company, USA) under air atmosphere. The crystal type was analyzed by using X-ray diffractometer (D2, Bruker Germany). Meanwhile, the Debye–Scherrer formula is used to calculate the crystal size of ZnO [28]. The inner structure of HCNFs and HCNFs@ZnO was explored by Raman spectrometer (Model Lab RAM HR800, France) with 633-nm laser light. X-ray photoelectron spectrometer with Al K α radiation (Thermo

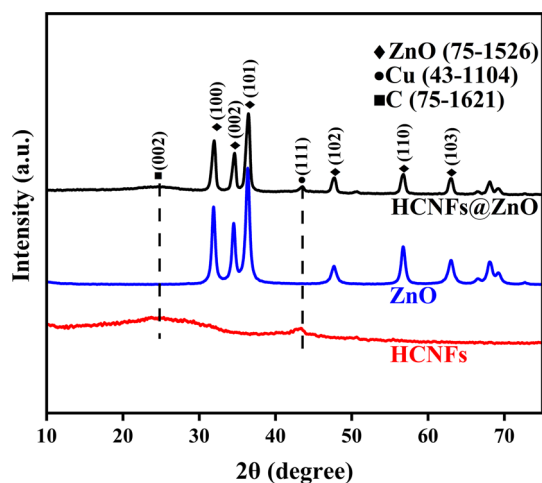
Table 1 Formulae of the NR composites, phr

Samples	c-ZnO/NR (5/100)	HCNFs/NR (control, 5/100)	HCNFs/NR (control, 10/100)	HCNFs@ZnO/NR (10/100)
c-ZnO	5	5	5	0
HCNFs	0	5	10	0
HCNFs@ZnO	0	0	0	10
NR	100	100	100	100
SA	3	3	3	3
DM	0.6	0.6	0.6	0.6
S	2.5	2.5	2.5	2.5
CB	50	50	50	50

Scientific) was used to analyze the surface composition and chemical valence of samples.

The vulcanization test was performed at 145 °C for 30 min using a mobile mold rheometer (GT-M2000-A, China). According to ISO 37:2011, the mechanical properties of rubber composites were tested on universal testing machine (RGM-50, China). The swelling index was determined by using the equilibrium swelling method, to express the crosslinking density of rubber [29].

Dynamic mechanical analysis instrument (Q800, USA) was used for dynamic mechanical analysis and testing at a frequency of 1 Hz, a temperature range of -80 °C to 80 °C, with the heating rate of 3 °C/min. Hardness of rubber was tested by Shore durometer (JLX-A, China).

**Figure 1** XRD spectra of HCNFs, ZnO, and HCNFs@ZnO.

Results and discussion

Characterization of HCNFs@ZnO hybrid

Figure 1 shows the XRD patterns of HCNFs, ZnO, and HCNFs@ZnO. In the curves for HCNFs@ZnO and ZnO, the characteristic peaks located at 31.8°, 34°, 36.3°, 47.5°, 56.6°, 62.9°, and those were a typical ZnO structure of the six-sided crystal (JCPDS: 36-1451). Moreover, the characteristic peaks located at 26° and 44° in the curves of HCNFs and HCNFs@ZnO can be assigned to hcp-C (JCPDS: 75-1621) and fcc-Cu (JCPDS: 04-0836), respectively. Noted that Cu was introduced in the synthesis procedure of HCNFs, in which Cu acts as a catalyst to promote the formation of HCNFs. In addition, the average crystal size of ZnO in HCNFs@ZnO is calculated to be 25.4 nm according to the Debye–Scherrer equation, which is lower than that of pure ZnO (39.2 nm). The result reveals that HCNFs have a distinct effect on inhibiting the grain growth of ZnO nanoparticles. According to the XRD pattern of HCNFs@ZnO, moreover, the mass ratio of HCNFs to ZnO is estimated to be 52:48 by using the quantitative analysis function of Jade 6.0 software (fitting error ≤ 6%) [30], which is close to the design mass ratio of HCNFs to ZnO (50:50).

Figure 2a, b shows the SEM morphologies of HCNFs and HCNFs@ZnO, respectively. HCNFs exhibit a distinct helical structure with a thickness of around 80 nm. For HCNFs@ZnO, many ZnO nanoparticles are uniformly embedded on the surface of the HCNFs. The TEM image is illustrated in Fig. 2c, the HCNFs matrix maintains the helical structure, while the ZnO nanoparticles are uniformly loaded on the HCNFs surface with an average size of 30 nm. As shown in Fig. 2d, the lattice fringes with an interplanar spacing of 0.281 nm and 0.162 nm can

Figure 2 SEM images of **a** HCNFs, **b** HCNFs@ZnO, and **c, d** TEM images of HCNFs@ZnO.

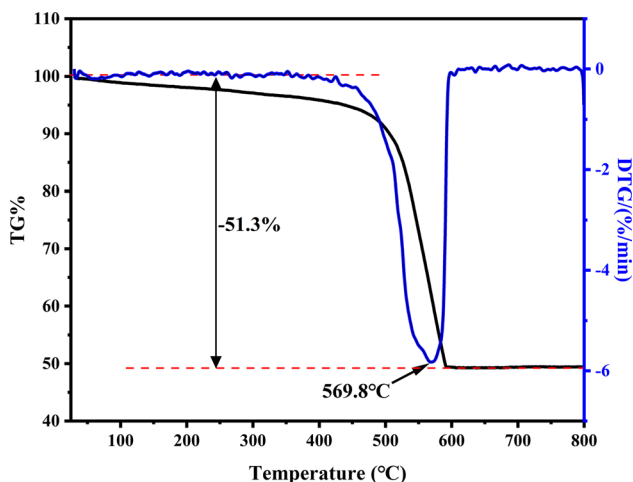
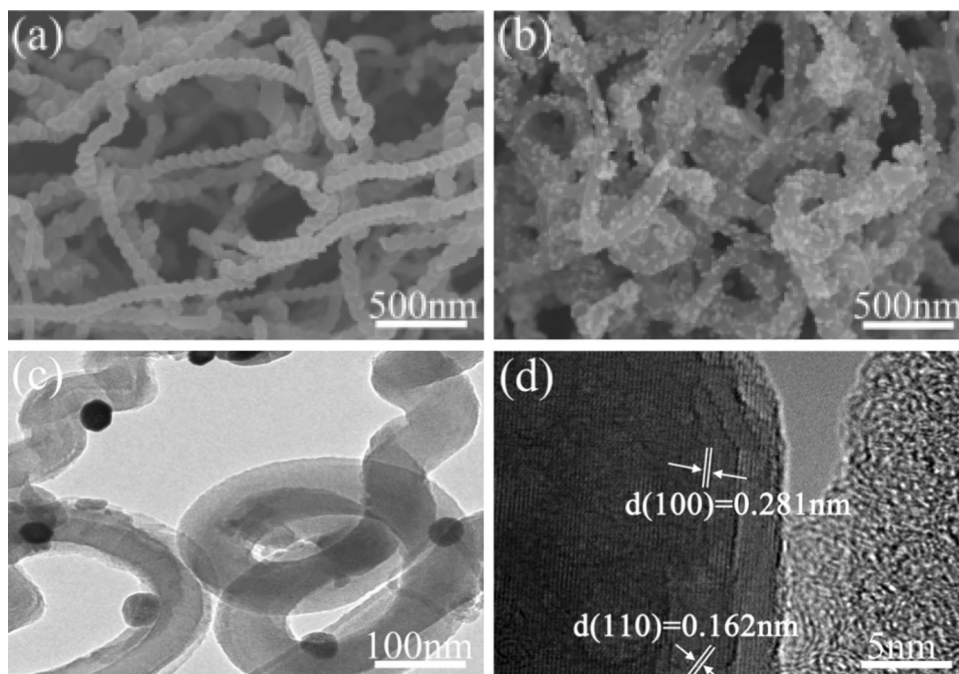


Figure 3 TG-DTG curves of HCNFs@ZnO from 25 to 800 °C.

be attributed to the (100) and (110) crystal planes of ZnO phase.

Figure 3 shows the thermogravimetric and differential thermal gravity curves of HCNFs@ZnO at air atmosphere in the range of RT to 800 °C. As seen in it, the weight loss of HCNFs@ZnO accelerates with the increasing temperature, and the biggest weight loss occurs at about 568.9 °C. More than 600 °C, TG and DTG curves become flat, indicating that HCNFs are entirely consumed by oxygen. Thus, it can be deduced that the HCNFs content in HCNFs@ZnO is 51.33 wt%, which is close to the XRD result.

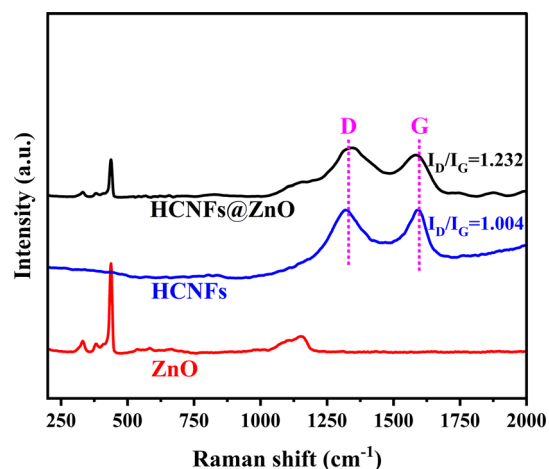


Figure 4 Raman spectra of ZnO, HCNFs, and HCNFs@ZnO.

Raman spectra were employed to further investigate the structure property of HCNFs@ZnO, as shown in Fig. 4. For HCNFs, there are two characteristic peaks located at 1322 cm^{-1} (D band) and 1573 cm^{-1} (G band), which correspond to the disordered graphitic carbon and the graphite carbon, respectively [31, 32]. Apart from these two characteristic peaks of carbon, HCNFs@ZnO also contains some characteristic peaks of ZnO. In addition, the I_D/I_G values of HCNFs and HCNFs@ZnO can be calculated to be 1.004 and 1.232, respectively, revealing that more defects are introduced into HCNFs during the synthesis of HCNFs@ZnO.

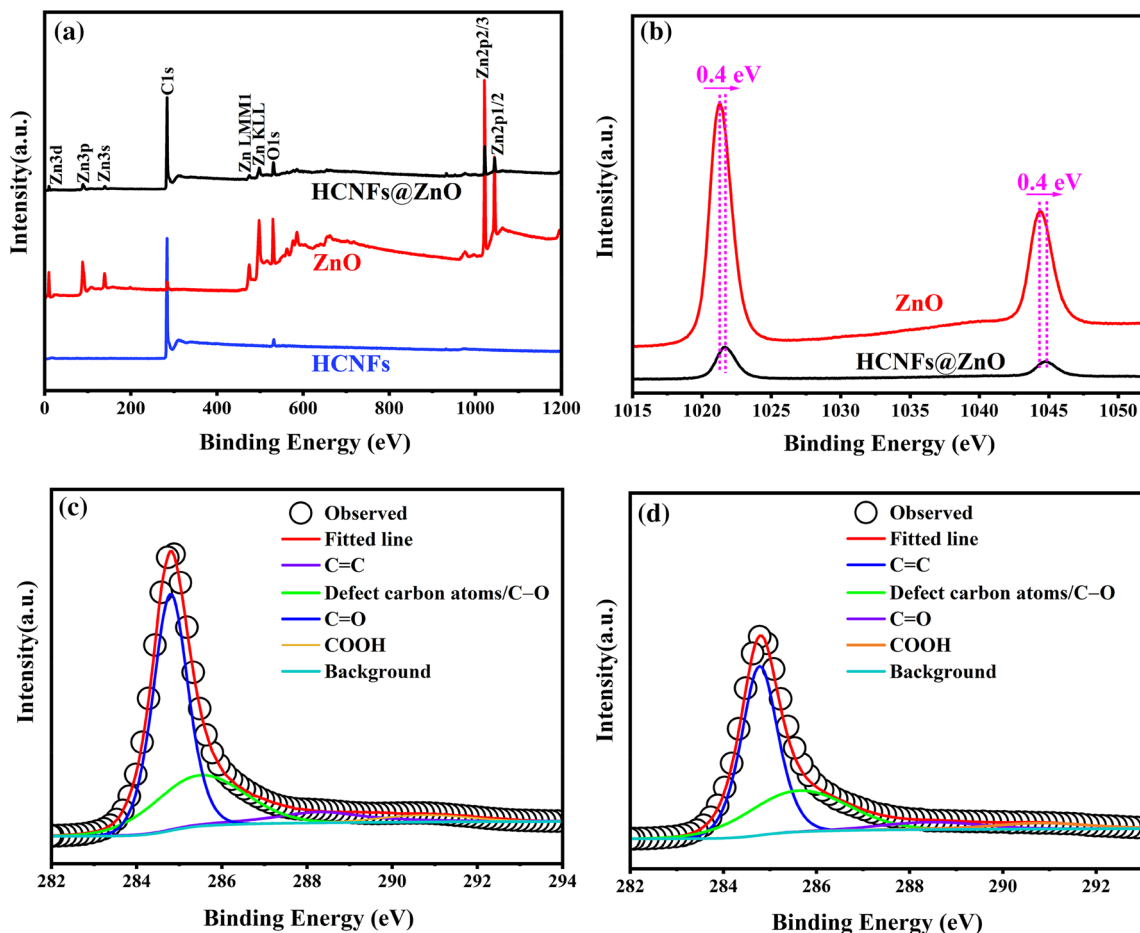


Figure 5 a XPS full spectra of HCNFs, ZnO, and HCNFs@ZnO; b Zn2p spectra of ZnO and HCNFs@ZnO; c C1s spectra of HCNFs; d C1s spectra of HCNFs@ZnO.

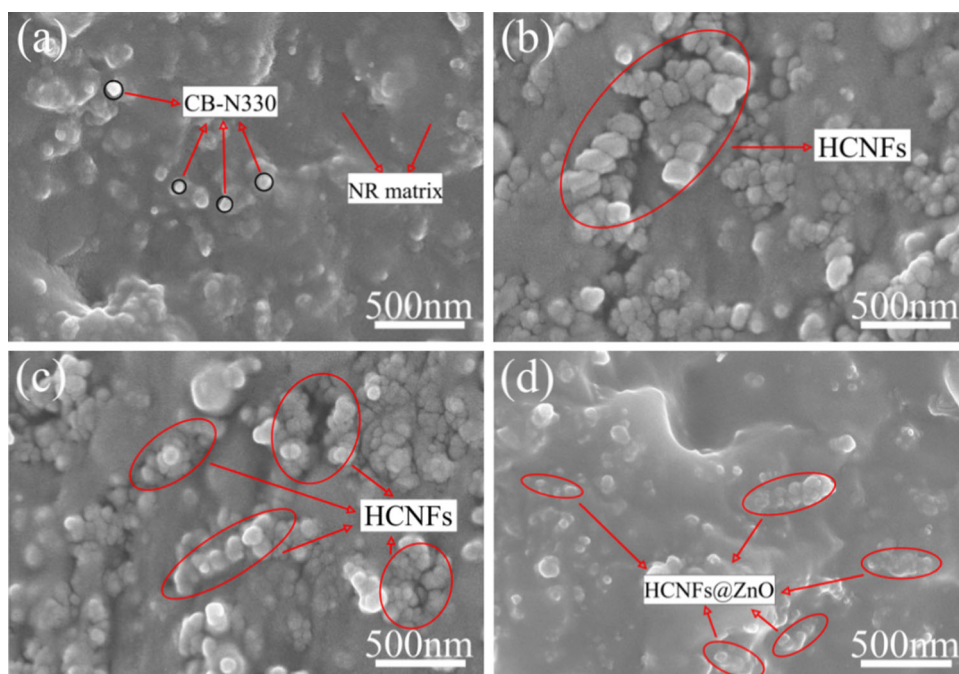
XPS was used to analyze the valence state and the structure information of HCNFs and HCNFs@ZnO, as shown in Fig. 5. As can be seen, elements C, Zn, and O present in HCNFs@ZnO (Fig. 5a). For HCNFs@ZnO, the high-resolution Zn 2p spectra (Fig. 5b) display the two characteristic peaks located at 1021.6 eV and 1044.6 eV, which arise from the contributions of Zn 2p_{3/2} and Zn 2p_{1/2}, respectively. Importantly, the binding energy of Zn 2p in HCNFs@ZnO shows a slight increase of 0.3 eV compared with that of pure ZnO. The positive shift of the binding energy of Zn 2p indicates that there is the

electron transport from ZnO to HCNFs due to the interface interaction between ZnO and HCNFs. Similar interfacial interactions and electron transport phenomena also appear in graphene/nitrogen, graphene/TiO₂, and C@TiO₂ [33–36]. The high-resolution C 1s spectra (Fig. 5c, d) exhibit four peaks located at 284.8, 285.6, 288.4, and 290.7 eV, corresponding to C–C/C=C, C–O, C=O, and COOH groups [37], respectively. The atomic contents of four carbon groups are listed in Table 2. Obviously, HCNFs@ZnO exhibits higher C–O, C=O, and COOH contents compared with pure HCNFs, which might

Table 2 The atomic content of carbon species in HCNFs and HCNFs@ZnO

Samples		C–C/C=C	C–O	C=O	COOH
HCNFs	BE value	284.8	286.0	288.5	290.8
	Content (at.%)	68.29	21.67	5.06	4.99
HCNFs@ZnO	BE value	284.8	286.0	288.5	290.8
	Content (at.%)	53.21	35.28	7.32	5.09

Figure 6 FESEM tensile fracture morphologies rubber composites with different additives. **a** c-ZnO/NR (5/100), **b** HCNFs/NR (5/100), **c** HCNFs/NR (10/100), and **d** HCNFs@ZnO/NR (10/100).



be due to the adsorption of corresponding functional groups by hydrolysis of the precursor [38].

Figure 6 shows the fracture cross-sectional morphologies of the as-prepared samples after the tensile test. Only some CB particles can be found in the rubber matrix for c-ZnO/NR composite (Fig. 6a). For HCNFs/NR (5/100) composite and HCNFs/NR (10/100) composite, the HCNFs show a high agglomeration phenomenon and mutual tangles (Fig. 6b, c), proving that single HCNFs hardly disperse evenly in the rubber matrix. For HCNFs@ZnO/NR composite, there is a good dispersion of HCNFs@ZnO in the NR composite (Fig. 6d). The results reveal that ZnO nanoparticles positively contribute to improving the disperse state of HCNFs in the rubber matrix. In addition, the fracture surface of a composite is rough and uneven, and HCNFs@ZnO is wrapped by rubber

matrix, which indicates that there is a strong interface effect between filler and rubber matrix.

Crosslinking characteristics of NR composites

The crosslinking characteristics of NR composites were tested on a torque rheometer. The vulcanization rate index (CRI) and the torque difference (MH-ML) are listed in Table 3, in which CRI is calculated according to the following formula [39]:

$$\text{CRI} = \frac{100}{T_{90} - T_{S2}} \quad (1)$$

where T_{90} is positive vulcanization time, and T_{S2} is scorch time.

The CRI value of HCNFs@ZnO/NR composite (7.31 min^{-1}) is about 1.40 times higher than that of

Table 3 Crosslinking characteristics of NR composites

Samples	c-ZnO/NR (5/100)	HCNFs/NR (control, 5/100)	HCNFs/NR (control, 10/100)	HCNFs@ZnO/NR (10/100)
T_{S2} (min)	2.49	2.39	2.44	1.54
T_{90} (min)	21.56	21.40	21.34	15.22
CRI (min^{-1})	5.24	5.26	5.29	7.31
M_L (dN m)	1.62	1.58	1.54	0.95
M_H (dN m)	15.91	16.38	16.56	17.61
$M_H - M_L$ (dN m)	14.29	14.80	15.02	16.66

c-ZnO/NR composite, revealing that HCNFs@ZnO/NR composite has a higher vulcanization rate. Moreover, the contribution of HCNFs to CRI is found to be tiny. Thus, it could be concluded that the improved CRI value for HCNFs@ZnO/NR composite mainly comes from the contribution of ZnO nanoparticles. Comparing with that of c-ZnO/NR composite, the maximum torque value (M_H) is increased by 16.59% for HCNFs@ZnO/NR composite, which indicates a better cure state of HCNFs@ZnO than c-ZnO. At the same time, the difference between maximum and minimum torques ($M_H - M_L$) also increases from 14.29 to 16.66 dN m with the addition of HCNFs@ZnO. As is well known, the value of $M_H - M_L$ is directly proportional to the crosslinking density [40]. Among these four fillers, therefore, HCNFs@ZnO is the most effective filler to improve the crosslinking effect of NR matrix.

Figure 7 shows the swelling index results of NR composites with HCNFs and HCNFs@ZnO additives. The lower the swelling index is, the higher the crosslinking density is [29]. Notably, the swelling index has a tiny decrease after the addition of HCNFs. When HCNFs@ZnO is added, the swell index reaches the lowest value of 2.29, meaning a highest degree of crosslinking. Therefore, it can be concluded that HCNFs@ZnO is conducive to improving vulcanization rate and crosslinking density.

Dynamic mechanical properties of NR composites

Figure 8 shows the storage modulus (E') and the loss modulus (E'') curves of the NR composites. E' is

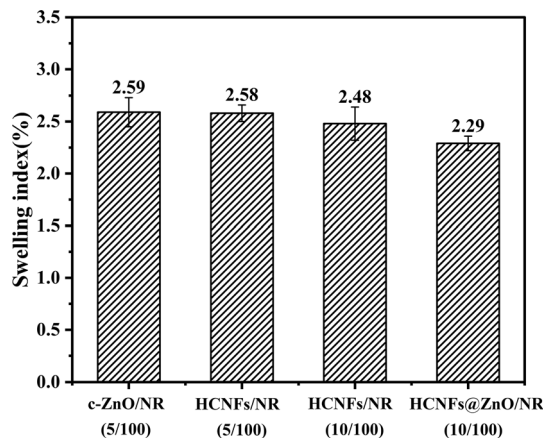


Figure 7 The swelling index of NR composites.

proportional to the maximum elasticity stored in the rubber sample in each cycle, reflecting the elastic component in the viscoelastic rubber. E'' is related to the energy consumed by the rubber sample in each cycle, reflecting the viscosity component in the rubber viscoelasticity [41, 42]. As shown in Fig. 8a, the E' of HCNFs@ZnO/NR composite is higher than c-ZnO/NR and HCNFs/NR composite. The result reveals that HCNFs@ZnO can improve the vulcanizate stored energy and resilience at low temperature, which is crucial for rubber's safety in some extreme weather condition. As the temperature rises, the rubber segments begin to become soft and the rubber rigidity decreases gradually, resulting in the decline of E' [43, 44]. Moreover, HCNFs/NR composite shows a higher E' value than c-ZnO/NR on account for a strong interfacial interface between HCNFs and NR matrix. Thus, the highest E' value of HCNFs@ZnO/NR composite should be ascribed to the accumulated contribution of HCNFs and ZnO nanoparticles.

As shown in Fig. 8b, the E'' of HCNFs@ZnO/NR composite is much higher than other NR composites in the range of -80 to -40 °C. As is well known, higher E'' means larger viscosity deformation and bigger contact area, thereby enhancing the driving safety of vehicles [45]. In addition, HCNFs@ZnO/NR exhibits the lowest E'' in the range of 40 – 80 °C, revealing a lowest thermogenesis among four NR composites. HCNFs@ZnO/NR composite is believed to achieve the long service lifetime at high-temperature area.

Figure 9a shows the $\tan\delta$ –temperature curves of NR composites. Generally, the internal friction value ($\tan\delta$) at 0 °C is used to evaluate the wet-skid resistance, while $\tan\delta$ at 60 °C represents the rolling resistance [18, 42]. For conventional rubber composites, it is found that the rolling resistance increases at expense of the wet-skid resistance, and vice versa. The $\tan\delta$ value of HCNFs@ZnO/NR composite at 0 °C is 0.1183, surpassing those of c-ZnO/NR (0.1047), HCNFs/NR (5/100) (0.1128), and HCNFs/NR (10/100) composite (0.1108). Interestingly, the $\tan\delta$ value of HCNFs@ZnO/NR at 60 °C (0.0905) is lower than those of c-ZnO/NR (0.1124), HCNFs/NR (5/100) (0.1065), and HCNFs/NR composite (10/100) (0.1035). It is obvious that HCNFs@ZnO/NR simultaneously improves rolling resistance and wet-skid resistance due to its better interfacial interaction.

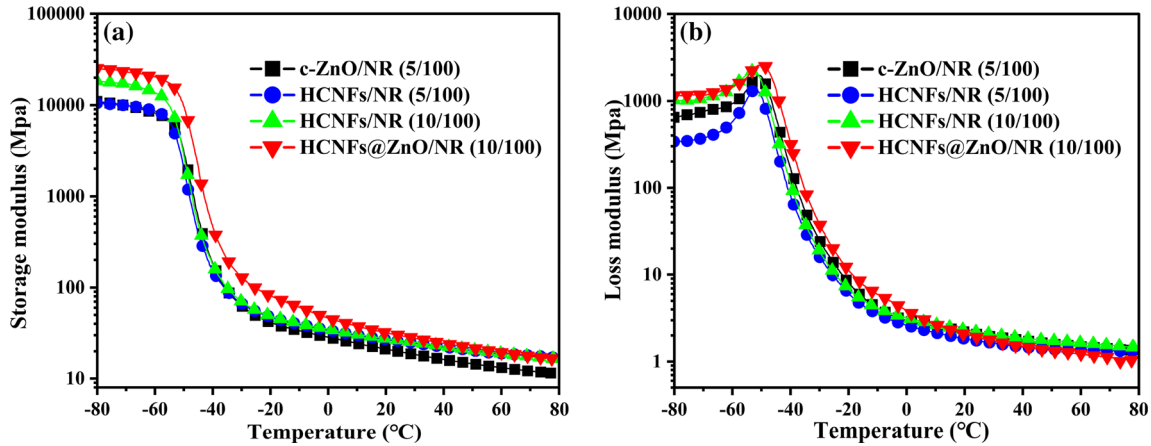


Figure 8 a Storage modulus versus temperature curve of NR composites, and b loss modulus versus temperature curve of NR composites.

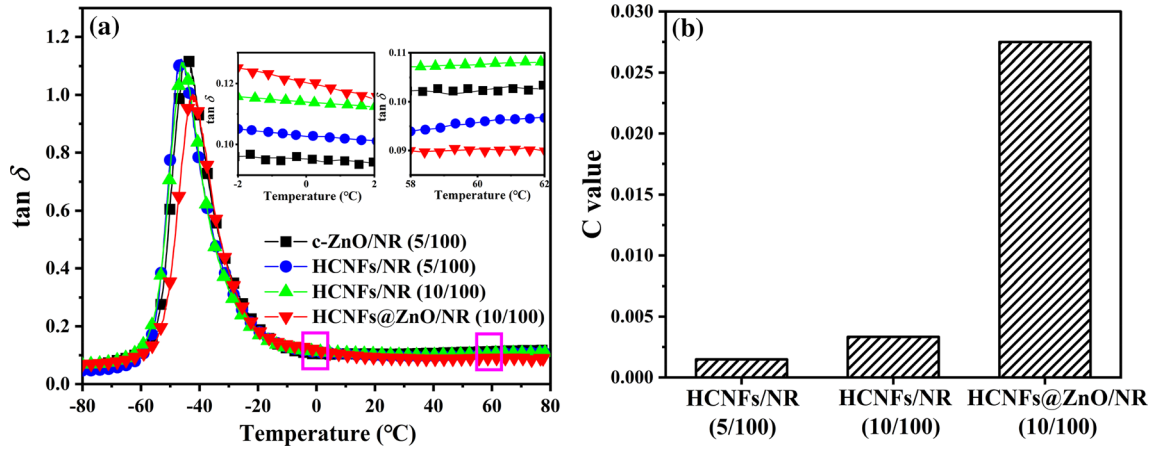


Figure 9 a Loss factor versus temperature curve and b constrained rubber matrix of NR composites.

The constrained rubber matrix (*C*) is introduced to quantitatively describe the interfacial interaction, which can be characterized by the following formula [46, 47]:

$$W = \frac{\pi \tan \delta}{\pi \tan \delta + 1} \tag{2}$$

$$C = 1 - \frac{(1 - C_0)W}{W_0} \tag{3}$$

where *W* is specified as the energy loss fraction of rubber, and *W*₀ and *C*₀ are specified as energy loss fraction of constrained rubber and the volume fraction in the *c*-ZnO/NR composite, respectively. Herein, *C*₀ is defined as 0, i.e., the *C* value of *c*-ZnO/NR composite equals to 0. As shown in Fig. 9b, the *C* value of the HCNFs@ZnO/NR composite is 0.0275, which is 18.33 and 8.33 times higher than those of HCNFs/NR (5/100) composite and HCNFs/NR (10/100) composite. This result reveals that the

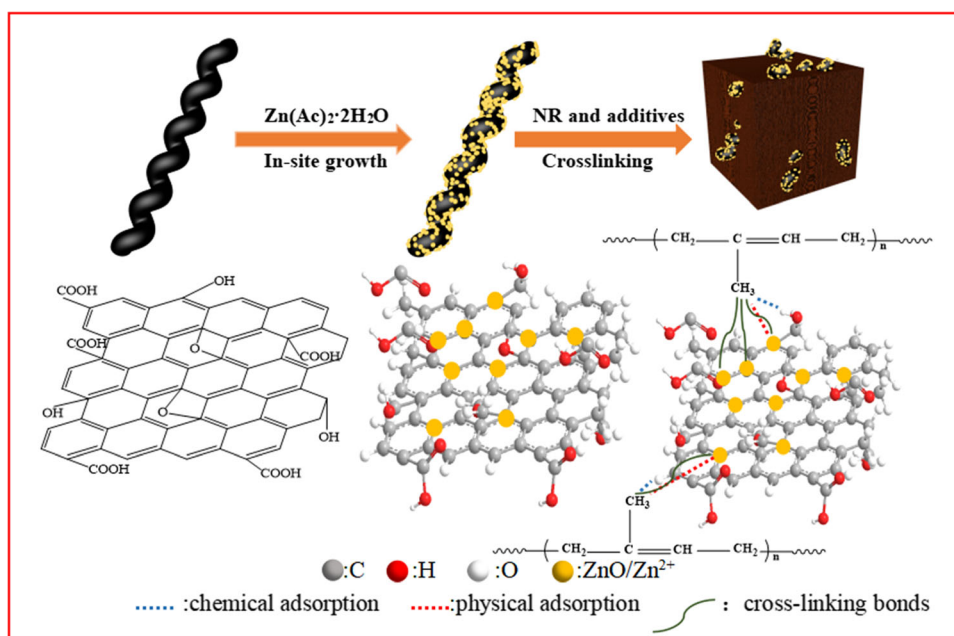
HCNFs@ZnO/NR composite shows the highest interfacial interaction between HCNFs@ZnO and NR. Meanwhile, the enhanced interfacial interaction should mainly ascribe to the ZnO nanoparticles in HCNFs@ZnO.

Mechanical properties of NR composites

The mechanical properties of NR composites are listed in Table 4. Compared with the *c*-ZnO/NR composite, the tensile strength, elongation at break, modulus at 300% elongation, and shore hardness of the HCNFs@ZnO/NR composite increase by 14%, 11%, 6%, and 5%, respectively. In addition, HCNFs/NR (5/100) and HCNFs/NR (10/100) exhibit the better comprehensive mechanical properties than *c*-ZnO/NR, indicating that the HCNFs can also act as an effective reinforcement. It is pointed that with respect of the mechanical properties, HCNFs/NR

Table 4 Mechanical properties of NR composites

Samples	c-ZnO/NR (5/100)	HCNFs/NR (control, 5/100)	HCNFs/NR (control, 10/100)	HCNFs@ZnO/NR (10/100)
Tensile strength (MPa)	21.08 ± 0.42	21.73 ± 0.40	20.95 ± 0.78	24.04 ± 0.89
Elongation at break (%)	424.18 ± 4.38	442.67 ± 4.00	445.83 ± 4.31	470.20 ± 5.33
Modulus at 300% elongation (MPa)	13.12 ± 0.25	13.25 ± 0.28	13.43 ± 0.21	13.89 ± 0.21
Hardness (Shore A)	70.07 ± 0.50	70.18 ± 0.78	72.47 ± 0.60	73.77 ± 0.4

Figure 10 Schematic of interaction in HCNFs@ZnO and NR composites.

cannot hold a candle to HCNFs@ZnO/NR. In a word, HCNFs@ZnO provides a stronger reinforcing effect in mechanical properties of NR composites than c-ZnO and pure HCNFs.

As shown in Fig. 10, the excellent mechanical properties of HCNFs@ZnO/NR can be better understood from the following aspects: (1) There is a vital interface interaction between the HCNFs and nano-ZnO, which significantly improves the dispersion of nanoscale ZnO in the NR matrix; (2) a large amount of Zn^{2+} anchor on the surface of HCNFs and form metal–ligand coordination bonds; then, these Zn^{2+} can bridge the HCFs and NR molecules; (3) compared to C-ZnO, ZnO nanoparticles in HCNFs@ZnO have larger specific surface area and provide more active sites to react with S, resulting in higher vulcanization rate and crosslinking density.

Conclusion

In summary, helical carbon nanofiber-supported ZnO nanoparticles (HCNFs@ZnO hybrid) were synthesized via a simple in situ growth method. As a nanofiller, HCNFs@ZnO hybrid can improve effectively the vulcanization rate and the crosslinking density of NR composite. Compared with c-ZnO/NR composite, HCNFs@ZnO/NR composite displays a higher vulcanization rate index (7.31 min^{-1} vs. 5.25 min^{-1}) and a smaller swelling index (2.29% vs. 2.39%) due to synergistic effect of HCNFs and ZnO. Meanwhile, tensile strength, elongation at break, and modulus at 300% elongation of HCNFs@ZnO/NR composite increase by 14%, 11%, and 6%, respectively. In addition, HCNFs@ZnO/NR composite also shows higher wet-skid resistance and lower rolling resistance. Therefore, HCNFs@ZnO hybrids could be

a promising nanofiller for high-performance nature rubber composite.

Acknowledgements

The authors gratefully acknowledge the financial support from the National Natural Science Foundation of China (51572177, 51764017) and the Innovation Fund of Postgraduate, Sichuan University of Science & Engineering (D10501273).

Declarations

Conflict of interest The authors declared that there is no conflict of interest.

Supplementary Information: The online version contains supplementary material available at <http://doi.org/10.1007/s10853-021-06612-8>.

References

- [1] Yoon BY, Kim JY, Hong U, Oh MK, Kim M, Han SB, Nam JD, Suhr J (2020) Dynamic viscoelasticity of silica-filled styrene-butadiene rubber/polybutadiene rubber (SBR/BR) elastomer composites. *Compos Part B* 187:107865
- [2] Cheng SS, Duan XY, Zhang ZY, An D, Zhao GZ, Liu YQ (2021) Preparation of a natural rubber with high thermal conductivity, low heat generation and strong interfacial interaction by using NS-modified graphene oxide. *J Mater Sci* 56:4034–4050. <https://doi.org/10.1007/s10853-020-05503-8>
- [3] Yu WW, Xu WZ, Xia JH, Wei YC, Luo MC (2020) Toughening natural rubber by the innate sacrificial network. *Polymer* 194:122419
- [4] Nair CP, Manshad PK, Ashir AM, Athul S (2020) Synthesis of 3-carbonyl acrylic acid-functionalized polystyrene and an insight in to its role in cross linking and grafting of polystyrene on to natural rubber. *Eur Polym J* 131:109688
- [5] Andideh M, Ghoreishy MH, Soltani S, Sourki FA (2021) Surface modification of oxidized carbon fibers by grafting bis (triethoxysilylpropyl) tetrasulfide (TESPT) and rubber sizing agent: application to short carbon fibers/SBR composites. *Compos Part A* 141:106201
- [6] Zhu QQ, Wang ZH, Zeng H, Yang T, Wang XX (2021) Effects of graphene on various properties and applications of silicone rubber and silicone resin. *Compos Part A* 142:106240
- [7] Roy K, Alam MN, Mandal SK, Debnath SC (2014) Surface modification of sol–gel derived nano ZnO (ZnO) and the study of its effect on the properties of styrene–butadiene rubber (SBR) nanocomposites. *J Nanostruct Chem* 4:133–142
- [8] Ibarra L, Alzorri M (2015) Vulcanization of carboxylated nitrile rubber (XNBR) by a mixed zinc peroxide-sulphur system. *Polym Int* 49:115–121
- [9] Susanna A, Armelao L, Callone E, Dirè S, Arienzoa Md, Credicoa BD, Giannini L, Hanel T, Morazzonia F, Scotti R (2015) ZnO nanoparticles anchored to silica filler. A curing accelerator for isoprene rubber composites. *Chem Eng J* 275:245–252
- [10] Jacna VC, Ramesan MT (2018) Fabrication of novel nanocomposites from styrene-butadiene rubber/zinc sulphide nanoparticles. *J Mater Sci* 53:8250–8262. <https://doi.org/10.1007/s10853-018-2173-z>
- [11] Thomas SP, Mathew EJ, Marykutty CV (2012) Synthesis and effect of surface modified nano ZnO in natural rubber vulcanization. *J Appl Polym Sci* 124:3099–3107
- [12] Mostoni S, Milana P, Credico BD, Arienzo MD, Scotti R (2019) Zinc-based curing activators: new trends for reducing zinc content in rubber vulcanization process. *Catalysts* 9:664
- [13] Wei YC, Liu GX, Zhang L, Zhao F, Liao S, Luo MC (2020) Exploring the unique characteristics of natural rubber induced by coordination interaction between proteins and Zn²⁺. *Polymer* 193:122357
- [14] Wang R, Xie CZ, Zeng LL, Xu HS (2019) Thermal decomposition behavior and kinetics of nanocomposites at low-modified ZnO content. *RSC Adv* 9:790–800
- [15] Panampilly B, Thomas S (2013) Nano ZnO as cure activator and reinforcing filler in natural rubber. *Polym Eng Sci* 53:1337–1346
- [16] Maiti M, Basak GC, Srivastava VK, Jasra RV (2017) Influence of synthesized nano-ZnO on cure and physico-mechanical properties of SBR/BR blends. *Int J Ind Chem* 8:273–283
- [17] Qin X, Xu HS, Zhang GG, Wang JD (2020) Enhancing the performance of rubber with nano ZnO as activators. *ACS Appl Mater Interfaces* 12:48007–48015
- [18] Liang YH, Liu XL, Wang LL, Sun JT (2017) The fabrication of microcrystalline cellulose-nanoZnO hybrid composites and their application in rubber compounds. *Carbohydr Polym* 169:324–331
- [19] Xu ZC, Zheng L, Wen SP, Liu L (2019) Graphene oxide-supported zinc oxide nanoparticles for chloroprene rubber with improved crosslinking network and mechanical properties. *Compos Part A* 124:105492

- [20] Mittal G, Dhand V, Rhee KY, PSJ, Lee WR (2015) A review on carbon nanotubes and graphene as fillers in reinforced polymer nanocomposites. *J Ind Eng Chem* 21:11–25
- [21] Xu ZC, Jerrams S, Guo H, Zhou YF, Jiang L, Gao YY, Zhang LQ, Liu L, Wen SP (2020) Influence of graphene oxide and carbon nanotubes on the fatigue properties of silica/styrene-butadiene rubber composites under uniaxial and multiaxial cyclic loading. *Int J Fatigue* 131:105388
- [22] Raghubanshi H, Dikio ED, Naidoo EB (2016) The properties and applications of helical carbon fibers and related materials: a review. *J Ind Eng Chem* 44:23–42
- [23] Shaikjee A, Coville NJ (2012) The synthesis, properties and uses of carbon materials with helical morphology. *J Adv Res* 3:195–223
- [24] Hu JT, Zhao TK, Peng XR, Yang WB, Ji XL, Li TH (2018) Growth of coiled amorphous carbon nanotube array forest and its electromagnetic wave absorbing properties. *Compos B* 134:91–97
- [25] Jin YZ, Ren J, Chen J, Dai ZY, Li BH, Zhou XS (2017) Controllable preparation of helical carbon nanofibers by CCVD method and their characterization. *Mater Res Express* 5:015601
- [26] Zheng XL, Jin YZ, Chen J, Li BH, Fu QS, He G (2019) Mechanical properties and microstructure characterization of natural rubber reinforced by helical carbon nanofibers. *J Mater Sci* 54:12962–12970. <https://doi.org/10.1007/s10853-019-03771-7>
- [27] Jin YZ, Zheng XL, Wang L, Chen J, Wang C, Li BH (2020) Improved mechanical properties of natural rubber composites reinforced by novel SiO₂@HCNFs nanofillers at a low filler loading. *J Appl Polym Sci* 137:49225
- [28] Mustapha S, Ndamits MM, Abdulkareem AS, Tijani JO, Shuaib DT, Mohammed AK, Sumaila A (2019) Comparative study of crystallite size using Williamson-Hall and Debye-Scherrer plots for ZnO nanoparticles. *Adv Nat Sci* 10:045013
- [29] Taib MN, Yehye WA, Julkapli NM (2019) Influence of crosslinking density on antioxidant nanocellulose in biodegradation and mechanical properties of nitrile rubber composites. *Fibers Polym* 20:165–176
- [30] Hillier S (2000) Accurate quantitative analysis of clay and other minerals in sandstones by XRD: comparison of a Rietveld and a reference intensity ratio (RIR) method and the importance of sample preparation. *Clay Miner* 35:291–302
- [31] Eckmann A, Felten A, Mishchenko A, Britnell L, Krupke R, Novoselov K, Casiraghi C (2012) Probing the nature of defects in graphene by Raman spectroscopy. *Nano Lett* 12:3925–3930
- [32] Ferrari AC, Meyer JC, Scardaci V, Casiraghi C, Lazzeri M, Mauri F, Piscanec S, Jiang D, Novoselov KS, Roth S, Geim AK (2006) Raman spectrum of graphene and graphene layers. *Phys Rev Lett* 97:187401
- [33] Sagadevan S, Pal K, Chowdhury ZZ, Foley M (2017) Controllable synthesis of graphene/ZnO-nanocomposite for novel switching. *J Alloys Compd* 728:645–654
- [34] Ramadoass A, Kim SJ (2013) Facile preparation and electrochemical characterization of graphene/ZnO nanocomposite for supercapacitor applications. *Mater Chem Phys* 140:405–411
- [35] Gao JP, Qiu GJ, Li HJ, Li MJ, Li CP, Qian LR, Yang BH (2020) Boron-doped graphene/TiO₂ nanotube-based aqueous lithium-ion capacitors with high energy density. *Electrochim Acta* 329:135175
- [36] Kumar R, Singh BK, Soam A, Parida S (2020) In situ carbon-supported titanium dioxide (ICS-TiO₂) as an electrode material for high performance supercapacitors. *Nanoscale Adv* 2:2376–2386
- [37] Wang L, Jin YZ, Chen J, Gong Y, Fang Y, Ren J (2019) Grafting of silica nanoparticles on incompletely-graphitized HCNFs for application in bound rubber. *Chem Phys Lett* 717:124–129
- [38] Zhang Q, Tian CJ, Wu AP, Tan TX (2012) A facile one-pot route for the controllable growth of small sized and well-dispersed ZnO particles on GO-derived graphene. *J Mater Chem* 22:11778–11784
- [39] Hadi FA, Kadhim RG (2019) Study of the effect of nano ZnO on cure characteristics and mechanical properties of rubber composites. *J Phys Conf Ser* 1234:12043
- [40] Nakanishi Y, Mita K, Yamamoto K, Ichino K, Takenaka M (2021) Effects of mixing process on spatial distribution and coexistence of sulfur and zinc in vulcanized EPDM rubber. *Polymer* 218:123486
- [41] Choi JH, Ryu JH, Kim SY (2010) Storage modulus of polybutadiene core in acrylonitrile-butadiene-styrene polymers with different degrees of grafting. *J Appl Polym Sci* 81:924–930
- [42] Tarawneh MA, Chen RS, Ahmad SH, Tarawni M, Saraireh S (2019) Hybridization of a thermoplastic natural rubber composite with multi-walled carbon nanotubes/silicon carbide nanoparticles and the effects on morphological, thermal, and mechanical properties. *Polym Compos* 40:695–703
- [43] Hu XL, He RZ, Huang YJ, Yin BY, Luo WB (2019) A method to predict the dynamical behaviors of carbon black filled natural rubber at different temperatures. *Polym Test* 79:106067
- [44] Sumita M, Tsukihi H, Miyasaka K (1984) Dynamic mechanical properties of polypropylene composites filled with ultrafine particles. *J Appl Polym Sci* 29:1523–1530
- [45] Thongnuanchan B, Ninjan R, Kaesaman A, Nakason C (2015) Studies on the ambient temperature crosslinking of

latex films based on natural rubber grafted with poly(diace-tone acrylamide) using DMTA. *J Polym Res* 22:1–11

- [46] Zhang X, Loo LS (2009) Study of glass transition and reinforcement mechanism in polymer/layered silicate nanocomposites. *Macromolecules* 42:5196–5207
- [47] Lin Y, Liu S, Peng J, Liu L (2016) The filler-rubber interface and reinforcement in styrene butadiene rubber composites

with graphene/silica hybrids: a quantitative correlation with the constrained section. *Compos A* 86:19–30

Publisher's Note Springer Nature remains neutral with regard to jurisdictional claims in published maps and institutional affiliations.